THE JOURNAL OF PHYSICAL CHEMISTRY B

Article

pubs.acs.org/JPCB

Local Frustration Determines Molecular and Macroscopic Helix Structures

Christopher J. Forman,*[,†] Szilard N. Fejer,[‡] Dwaipayan Chakrabarti,[†,§] Paul D. Barker,[†] and David J. Wales[†]

[†]Department of Chemistry, University of Cambridge, Lensfield Road, Cambridge CB2 1EW, U.K.

[‡]Department of Chemical Informatics, Faculty of Education, University of Szeged, Boldogasszony sgt. 6, Szeged 6725, Hungary and Pro-Vitam Ltd., str. Muncitorilor nr. 16, Sf. Gheorghe 520032, Romania

[§]Department of Chemistry, Indian Institute of Technology Delhi, Hauz Khas, New Delhi 110 016, India

Supporting Information

ABSTRACT: Decorative domains force amyloid fibers to adopt spiral ribbon morphologies, as opposed to the more common twisted ribbon. We model the effect of decorating domains as a perturbation to the relative orientation of β strands in a bilayered extended β-sheet. The model consists of minimal energy assemblies of rigid building blocks containing two anisotropic interacting ellipsoids. The relative orientation of the ellipsoids dictates the morphology of the resulting assembly. Amyloid structures derived from experiment are consistent with our model, and we use magnets to demonstrate that the frustration principle is scale and system independent. In contrast to other models of amyloid, our model isolates the effect of frustration from the fundamental interactions between building blocks to reveal the frustration rather than dependence of morphology on the physical interactions. Consequently, amyloid is viewed as a discrete molecular version of the more general macroscopic frustrated bilayer that is exemplified by Bauhinia seedpods. The model supports the idea that the interactions arising from an arbitrary peptide sequence can support an amyloid structure if a bilayer can form first, which suggests that supplementary protein sequences, such as chaperones or decorative domains, could play a significant role in stabilizing such bilayers and therefore in selecting morphology during nucleation. Our model provides a foundation for exploring the effects of frustration on higher-order superstructural polymorphic assemblies that may exhibit complex functional behavior. Two outstanding examples are the systematic kinking of decorated fibers and the nested frustration of the Bauhinia seedpod.

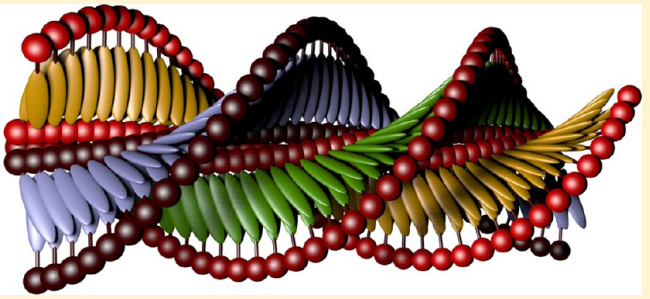

MOTIVATION AND INTRODUCTION

Many materials involve frustration, where part of a system cannot relax into its local ground state because of external constraints. Such frustration may induce interesting long- or short-range properties, which often give rise to complex emergent behavior. For example, tensegrity structures,[1−3] multidomain peptide structures,[4] amyloid fibers,[5,6] liquid crystals,[7] creased plates,[8] and bimetallic strips all exhibit internal frustration, which drives more complex behavior than any single component can exhibit alone.

In this work we use a well-known bilayer frustration principle, observed in Bauhinia seedpods,[9] to model an unexplained change in amyloid fiber morphology from a twisted to a spiral ribbon (see Figure 1). This transition was observed experimentally when a fiber-forming protein, SH3, was covalently linked to a second protein, cytochrome b_{562}.[10] On their own the SH3 domains typically form twisted ribbon amyloid fibres.[11,12] When combined with a cytochrome, the SH3−cytochrome b_{562} fusion proteins always formed fibers with a spiral ribbon morphology.[10,12]

Helical symmetry is very common, so it may be a coincidence that the fiber's morphological transition mimics the transition observed for the Bauhinia bilayers.[9] However, we note that known amyloid fiber structures in the literature, such as Aβ[13] and HET-s,[14] contain even numbers of β-sheets due to the hydrophobic inner surfaces packing against each other,[15] thus yielding a bilayered arrangement.

In the Bauhinia seedpods, the bilayer arrangement is fundamentally responsible for the helical morphologies, which minimize frustration between two stressed sublayers, each mutually inhibiting the other's relaxation.[9] Narrow strips cut from such frustrated bilayers, at specific angles relative to the internal stress, produce ribbons that adopt a helical morphology somewhere around the transition between twists and spirals (see Figure 1a−d).[9] Since the morphology depends on the cutting angle, the *shape* of the ribbon cannot be said to be a property of the material from which the bilayer is made.

Received: April 30, 2013

   dx.doi.org/10.1021/jp4040503 | J. Phys. Chem. B XXXX, XXX, XXX−XXX

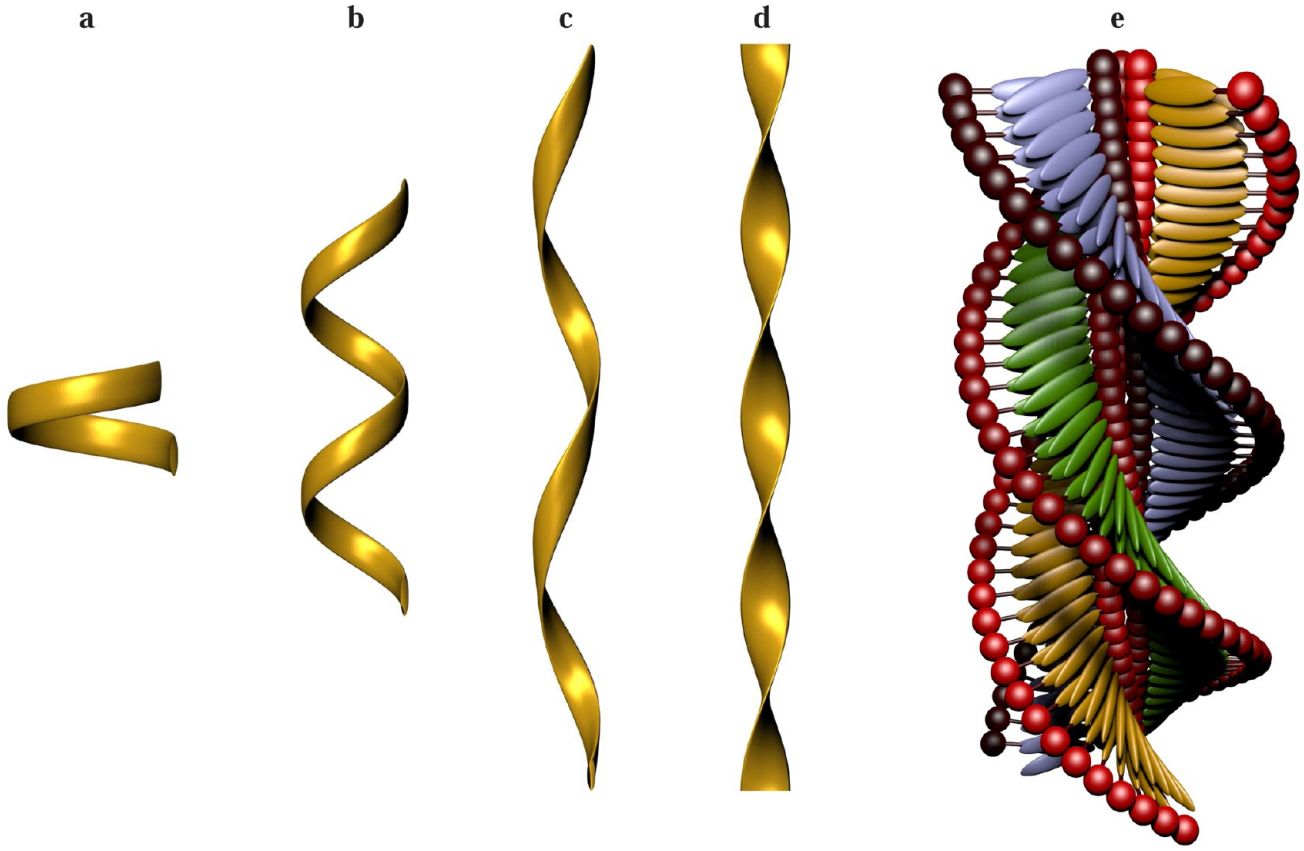

Figure 1. Range of morphologies available to a system with helical symmetry, such as an amyloid fiber. (a) A ring is the torsion free limit of helical morphology. This structure occurs in material cut from the bilayered Bauhinia seedpod when the cutting angle is parallel with the lines of stress in one of the layers of the bilayer (and perpendicular to the other).[9] (b) and (c) A spiral ribbon with nonzero curvature and torsion. In Bauhinia, the spiral morphology arises when the cutting angle is not extreme (i.e., not 0° or 45°).[9] (d) A twisted ribbon morphology, also known as a helicoid, arises in the Bauhinia bilayer when the cutting angle is at 45° to the internal lines of stress.[9] The central space curve of the ribbon is the vertical axis, which is the zero curvature limit of helical morphology. (e) A cartoon of an amyloid fiber consisting of three identical filaments, each in a spiral ribbon morphology. The β strands, represented by ellipsoids, are arranged in helical stacks to form the β sheet core of the fiber, in which the strands are approximately perpendicular to the central fiber axis (cross-β configuration). The red spheres represent material not involved in the helical core of the fibers. Such noncore material is responsible for causing a transition from a twisted ribbon morphology to a spiral ribbon morphology for the SH3−cytochrome b_{562} system considered in the text.

Instead, the morphology is an emergent property arising from geometric frustration between the bilayers. Indeed, any sufficiently elastic solid material has the potential to exhibit precisely this kind of behavior; for example, bimetallic strips curl when heated. Furthermore, as well as being material independent, frustration principles are also scale independent. Indeed, the recent use of DNA molecules to fabricate a tensegrity structure,[3] normally associated with the macroscopic regime,[2] demonstrates that the same frustration principle may be applied on multiple scales.

The transition of helical ribbons from twisted to spiral morphologies has been widely studied theoretically[16] and experimentally, from the shapes formed during laser−matter interactions[17] to the mechanical phase transitions in lipid springs.[18] Such helical symmetry arises whenever a translation and a rotation are coupled, which is readily achieved in numerous ways, including frustration[9] and molecular anisotropy.[19] The latter effect induces a twist in a linear stack of molecules so that the position and rotation of each molecule are correlated. Thus, helical symmetry is often defined in terms of twist angles between mutually adjacent components.[20]

A commonly used amyloid model employs anisotropically interacting rods that are free to rotate about their center of gravity, which assemble into sheets that stack together face-to-face.[20,21] The anisotropy of each rod drives twisting.[19] As the number of sheets increases the width of the fiber grows,[20−22] thereby increasing the required contour length of the outermost sheet. Consequently, in the outer sheets, the rods must be spaced further apart along their space curve; otherwise, they cannot be in-register with the innermost sheets. The outer sheets become increasingly unstable, and beyond the natural width limitation of around 5 nm the fibers undergo a transition to a crystalline phase.[15,20]

Such a model does not allow for the emergence of a spiral ribbon morphology, which is self-supporting with diameters as large as 30 nm.[12] The emergence of such a space curve is the principal difference between the decorated and undecorated fibers, so it is clear that the independent rod model is only adequate for short peptides that form twisted ribbons and must be revised to explain the effect of introducing the cytochrome. We note that the height of subfilaments in high-resolution atomic force microscopy (AFM) experiments, for both twisted and spiral morphologies, is typically 2−3 nm,[12] which is consistent with the width of bilayered subfilaments.[20,22,23]

Another approach to modeling amyloid is to reproduce spiral ribbons by directly changing the amphilicity and chirality of the

dx.doi.org/10.1021/jp4040503 | J. Phys. Chem. B XXXX, XXX, XXX−XXX

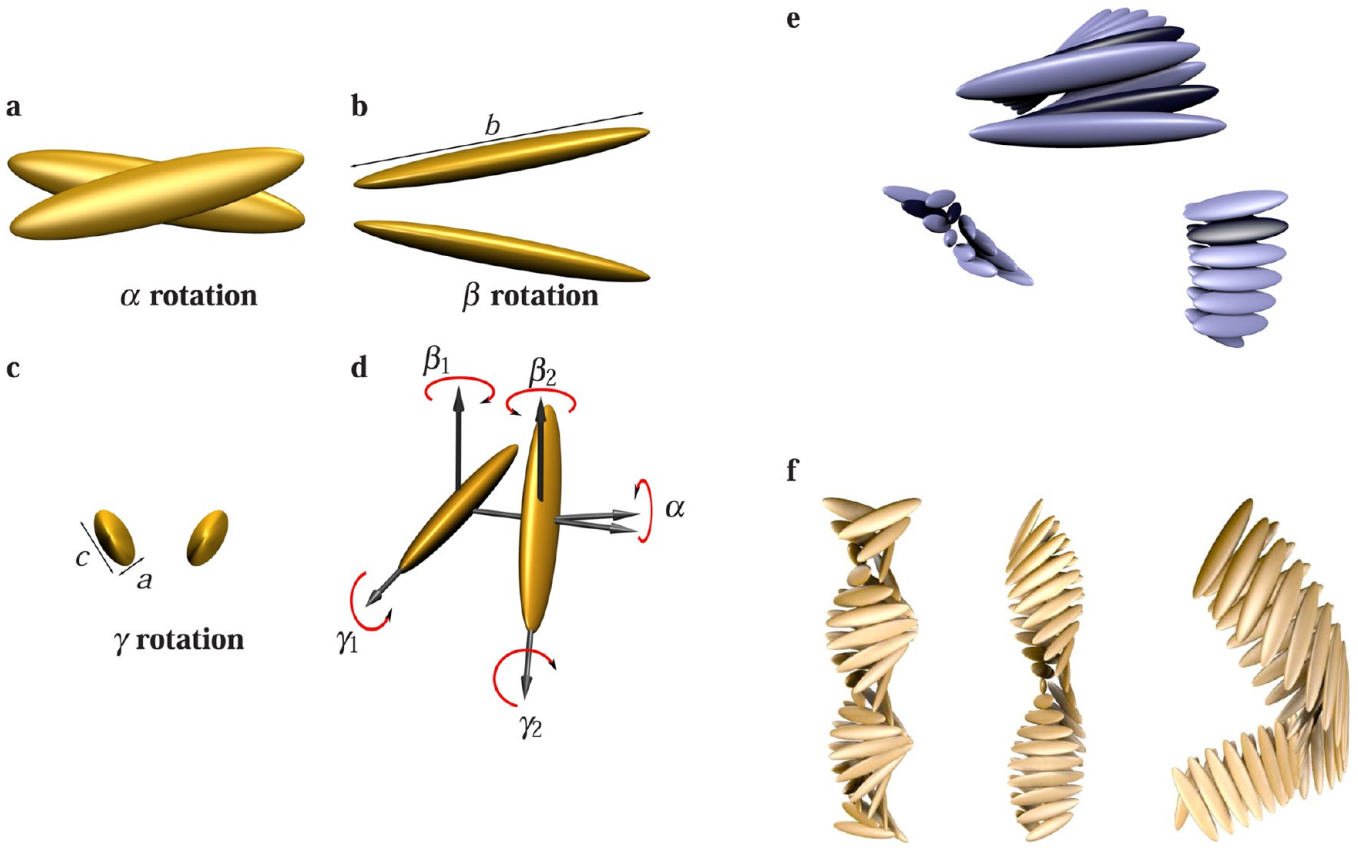

Figure 2. Two interacting anisotropic ellipsoids form a building block with specified displacement and relative orientation. (a) The angle of rotation about the line of centers (dihedral angle), α, is common to both ellipsoids and generates the "X"-shaped motif, whose chirality depends on the sign of α. (b) Each ellipsoid rotates about the lab frame z axis, through angles β_1 and β_2, thus defining a "V"-shaped motif when viewed from above. The ellipsoids' primary axis has length b. (c) Rotations about the longest body axis are labeled γ_1 or γ_2. Before rotation, the minor axes, labeled a and c, are aligned with the x axis and z axis, respectively. (d) All three rotations may be applied in the order: β, α (around the new a axis), and γ. More details can be found in the Supporting Information, Figure 1. (e) The linked pairs can be assembled in minimal energy arrangements, as shown in orthogonal views of the same group of six building blocks. The building block, colored in dark blue, consists of two sites that interact anisotropically[30] with sites in other building blocks. **(f)** The favored structures for aggregates of these building blocks are bilayer filaments, which exist in a continuum between twisted and cylindrically wound extremes, depending on the internal geometry of the building block. We consider only individual filaments in the present work rather than bundles of filaments.

underlying coarse-grained amino acid molecules.[24] However, this cannot explain how introducing a cytochrome could drive a transition from twisted to spiral morphologies because the cytochrome does not modify the chirality or amphilicity of the amino acids in the fiber-forming domain.

To develop a new model a coarse-grained representation of a decorated amyloid was generated, as depicted in Figure 1e, which illustrates a number of required features. The noncore material is shown as red spheres, and the cross-β structure of the multifilament core is depicted in terms of bilayered, helical stacks of ellipsoids arranged in a spiral ribbon, which have large helical space curves. In a real system there may be two or more filaments, which may exhibit domain swapping. Completely independent filaments could rotate about the common axis and stick together more closely, especially after adsorption on a surface, for example, during AFM or transmission electron microscopy (TEM).

Since frustration principles are independent of both scale and material, we ask: can the bilayered frustration operating in seedpods be transferred from a continuous macroscopic context to a discrete molecular picture, perhaps akin to the model in Figure 1e? If so, how could one manufacture such a molecular-scale bilayer? Could it be that such a model is an accurate description of both decorated and undecorated amyloid fibers and hence could explain the impact of introducing the cytochrome as a perturbation to the natural frustration experienced in such bilayers? This scenario would imply that amyloid *morphology* is not a property of the underlying protein, just as the morphology of Bauhinia ribbons is a consequence of the cutting angle of the Bauhinia bilayer rather than a fundamental property of the underlying cellulose.[9] In this case, amyloid could be viewed as a molecular scale bilayer made from protein, in much the same way that DNA can be used to assemble a molecular tensegrity structure.[3] This model would provide a natural rationale for the suggestion that any protein may form amyloid, regardless of sequence,[25] but only if the protein can form a bilayer first.

The approach we have taken to explore this question is to model β strands as interacting anisotropic units (ellipsoids) that are constrained in rigid pairs, as portrayed in Figure 2a–d, to form a single composite building block. The internal arrangements of the building block are indexed by the Euler angles of the ellipsoids, which we label α, β, and γ, as defined in Figure 2a, b, and c, respectively. The anisotropy of the ellipsoids defines the interaction potential between them and is represented by the lengths of the semiaxes denoted a, b, and

dx.doi.org/10.1021/jp4040503 | J. Phys. Chem. B XXXX, XXX, XXX–XXX

c (Figure 2). Minimal energy arrangements of such interacting rigid-body building blocks were then found using basin-hopping global optimization[26−28] employing the GMIN program.[29] The rigid pairs naturally form bilayered structures, in which each member of the pair is in a separate layer (Figure 2e). The resulting changes in the long-range morphology of the minimal energy structures due to the internal rearrangement of the building blocks (Figure 2f) were studied for a wide range of underlying anisotropies.

Ultimately, our model separates the effect of the tertiary structure from the effect of the interaction anisotropy on the long-range morphology. As anisotropic ellipsoids are useful models for β strands, the anisotropy of the ellipsoid models the amino acid sequence. Likewise, the internal angles of the rigid body emulate the tertiary structure of the protein, and the two kinds of information in the model—conformation represented as angles and sequence represented as anisotropy—can be varied independently.

The underlying energy landscape explored by global optimization corresponds to $2N$ individual ellipsoids, where N is the number of building blocks. Locking the ellipsoids into pairs restricts the accessible configurations. As expected, the global minima for assemblies of building blocks in this region of the landscape are bilayered forms, which reproduce the twisted ribbon to spiral ribbon morphology. Indeed the same bilayers and morphological transition are reproduced for a wide range of anisotropies that were estimated to bracket the anisotropies observed in β strands. This result is consistent with the idea that bilayered amyloid morphology is independent of the anisotropy of the β strands and therefore amino acid sequence.

As the energy barrier arising from bilayer formation, assumed to be driven by hydrophobic and other intersheet interactions in real fibers, can stabilize misfolded forms of the protein, our model is able to predict the changes in morphology that will arise due to the effect of the decorating payload and its linker on the internal frustration of the protein. These predictions would be prohibitively time-consuming for a fully atomistic representation, and our objective is to focus on generic properties, rather than any specific system. In the case of small peptide amyloids, where the sampling of conformation space is not affected by payloads or linkers but is highly sequence-dependent, such predictions are likely to require atomistic modeling and would be computationally very expensive, but here the independent rod model[20,21] would probably suffice.

The coarse-grained methodology employed here makes no assumptions about length scale, so it may be used to explore the same concept of frustration among discrete building blocks of any size with arbitrary interactions. We have validated this hypothesis experimentally by demonstrating the discrete bilayered principle for a stack of macroscopic magnetic particles, as described below.

Our model is consistent with the observation that frustration at both termini of a β strand inhibits stable fiber formation.[4] This result was observed experimentally when a cytochrome was appended to both termini of the SH3 fiber-forming domains. These dumbbell-like fusion proteins failed to form fibers under conditions in which fibers were observed for all other species of fusion protein.[12] Furthermore, the bilayered model is consistent with the kinetic formation mechanism of amyloid leading to polymorphism,[5,6,31] where the amyloid can adopt multiple morphologies in the same physicochemical environment. The model may also be adapted to explain the characteristic kinking of decorated amyloid fibers,[12] which hints at the possibility of higher-order behavior, potentially leading to novel routes for low energy bulk material formation and controlled dispersion of secondary nanoscale structures throughout a given volume, which is a significant challenge in industrial contexts.

Finally, we have analyzed two existing experimentally derived models of amyloid (Aβ and HET-s) as a further check for consistency between our model and experiment. The results for HET-s hint at the possibility of some interesting variations involving highly complex frustration mechanisms, which go beyond simple bilayers.

MODELING THE FRUSTRATION

The anisotropic interactions between the coarse-grained building blocks are modeled using an anisotropic potential function, which defines the shape of the attractive and repulsive terms as ellipsoids.[30] The interparticle forces also subsume solvent interactions. Eight parameters are needed to define the potential:[30] three control the anisotropy of the repulsive component, defined as the lengths of semiaxes of the ellipsoid; three control the attractive anisotropy in the same way; and one controls the overall range of the interaction. The eighth parameter sets the energy scale and is fixed. Two sites interacting via this soft potential exhibit a minimum energy at a center-to-center distance that varies smoothly with the relative orientation of the ellipsoids. The potential parameters are expressed in reduced units relative to the repulsion along the longest axis of the first ellipsoid. Only the repulsive ellipsoids are shown in the figures.

An appropriate choice of interaction parameters can be determined by considering the relative magnitude and direction of the forces for a β strand, which can be split into intra- and inter-β sheet terms. The values we considered are presented in Table 1 for two distinct choices, building block 1 (BB1) and building block 2 (BB2). Intrasheet interactions (c axis) consist of attractive hydrogen bonds and attractive or repulsive side-chain interactions. The intersheet potential (a axis) can be more complex and involves side-chain interactions such as salt bridges, solvent contributions, steric zippers, and van der Waals forces. BB1 has minor axes about one tenth of the major axis in length, in proportion to a ten-residue β strand. BB2 represents a shortened β strand with weaker attraction between the sheets. In reduced units, the length of the b axis is normalized to unity, so these changes for BB2 are introduced by *increasing* the relative interaction strength along the c axis. A full discussion

Table 1. Parameters for Two Choices of the Ellipsoidal Interaction Potential[30,a]

		a	b	c	σ_0	cutoff
BB1	repulsive	0.10	1.00	0.13	0.5	0.5
	attractive	0.04	0.10	0.14		
BB2	repulsive	0.09	1.00	0.20	0.2	0.5
	attractive	0.04	0.20	0.22		

[a]The column labelled a corresponds to the ellipsoid axis responsible for the intersheet interaction, while b corresponds to the end-to-end interactions. Axis c is responsible for the intrasheet interaction. The axis lengths are in reduced units. σ_0 is the range parameter of the interaction with respect to the ellipsoid dimensions, and the cutoff represents the separation between two ellipsoidal surfaces at which the potential smoothly vanishes.

dx.doi.org/10.1021/jp4040503 | J. Phys. Chem. B XXXX, XXX, XXX−XXX

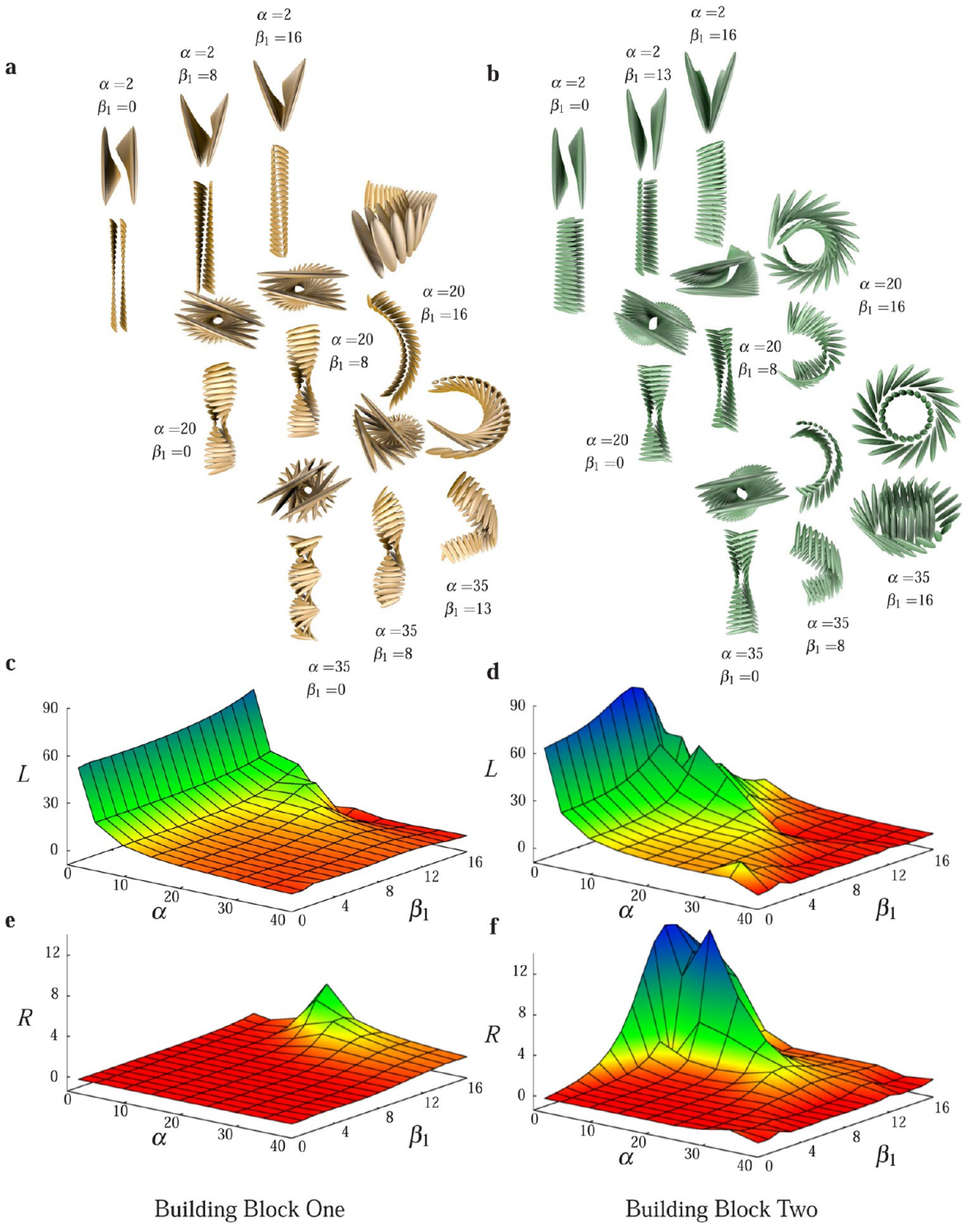

Figure 3. (a) Range of structures produced using BB1 by varying the internal parameters α and $\beta_1 = -\beta_2$. Varying α increases the amount of frustration between the bilayers, and varying β adjusts the resulting morphology. (b) Changing the building block potential does not qualitatively affect the response of the morphology to geometry. (c,d,e,f) The helical parameters (pitch length, L, and radius, R) of the structures can all be quantified and compared to produce a structural phase diagram that connects the internal geometry with the resulting morphology.

concerning our selection of parameters is included in the Supporting Information.

Having chosen the interaction potential for our building blocks we explored the resulting effective free energy landscape using global optimization[28] to identify low-energy structures. Adjusting only the internal geometry of the building block, we find that the favored morphology of a bilayered filament can lie anywhere on the continuum between twisted and spiral ribbons, as shown in Figure 3. The effect of adjusting only the angles α and β_1, while keeping $\beta_2 = -\beta_1$ and $\gamma_1 = \gamma_2 = 0$ for fixed interaction parameters, is illustrated in Figure 3a and b. Varying the γ angles did not reveal any new phenomenology.

Prior to energy minimization, stacks of identical building blocks were arranged to produce flat bilayers, which do not

dx.doi.org/10.1021/jp4040503 | J. Phys. Chem. B XXXX, XXX, XXX−XXX

a b c d

Figure 4. Magnetic "fibers" analogous to the computational model presented. (a) $\alpha = 0$, vertical stack; (b) $\alpha \approx 40°$, left-handed helix; (c) $\alpha > 45°$, left-handed helix with more twist than in (b); (d) $\alpha \approx -40°$, right-handed helix. Movies of the assembly and dynamics of these aggregates, demonstrating that they are minimal energy structures, are included in the Supporting Information, Movies S1−S5.

correspond to local minima. After minimization, the pitch length (torsion) and radius (curvature) of the resulting helical structures were quantified by tracing the position of a reference point within each building block to provide a reduced representation of the fiber geometry. We obtained the pitch length and radius of the resulting helices using standard fitting techniques,[32] and these values were employed to generate the surfaces illustrated in Figure 3 for helices traced out by the tip of the first ellipsoid in the building block.

Analyzing the curvature and torsion enables us to associate a particular continuum geometry[33] with a particular internal frustration, thereby providing a formal connection between the continuous morphology and the geometry of the discrete building blocks. The surfaces for varying pitch length (Figure 3c for BB1 and Figure 3d for BB2) are qualitatively similar, as are the surfaces for varying radius (Figure 3e and Figure 3f), differing principally in the precise position of peaks and transitions between different morphologies.

Results from basin-hopping global optimization[26−28] runs using the GMIN program[29] show that the BB1 helices are the global minima up to around $\beta_1 < 10°$ and $\alpha < 20°$. For BB2 the helices are low-lying local minima, and for larger angles the energy of the helices increases significantly. For example, with $\alpha = 45°$ and BB2 a spiral structure is a relatively high-energy local minimum. Nevertheless, when starting from a flat bilayer, the system consistently relaxes to a helical configuration on energy minimization.

If the geometric displacement between ellipsoids in each building block is purely dihedral ($\alpha \neq 0$, all other angles are zero), then a chiral X-shape motif is generated (Figure 2a). The structure twists and forms a helical filament, with a chirality that depends on the chirality of the building block itself. If the chirality of the tertiary structure can be controlled in this way, then long-range structures of either chirality can be produced, regardless of the chirality of the constituent amino acids, as observed experimentally for fibers[34] and also in the Bauhinia seedpods, where the two halves of the pod are both bilayers with opposite handedness.[9]

Starting from an X-shaped internal geometry, subsequent changes to $\beta_1 = -\beta_2$, which introduces a wedge or V shape into the building block (Figure 2b), can modify the amount of twisting. As the difference in β_1 and β_2 increases, eventually a maximum is reached and the structure changes to a ring-shaped geometry, with a low pitch length and a large radius. In the twisted ribbon morphologies the β strands are perpendicular to the fiber axis. As β increases, to yield increasingly cylindrically wound ribbons and ring shape morphologies, the angle between the β strands and the fiber axis also grows, a situation for which there is some experimental evidence in the case of α-Synuclein.[35]

The range of local minimum energy structures for BB1 and BB2 is consistent with the polymorphism observed experimentally for amyloid.[5,31,36] As oligomers form from individual proteins the precise cross-β geometry adopted could be frozen in and act as a template for further growth. Alternative morphologies are likely to be kinetically stable on an experimental time scale.

As well as reproducing basic experimental results, such as cross-β structure and polymorphism in amyloid, the applicability of our model to a macroscopic situation can be assessed by a simple experiment illustrated in Figure 4. The experiment demonstrates a macroscopic, yet *discrete*, frustrated bilayer in which magnetic building blocks were constructed from two uniaxial ellipsoidal magnets, with their poles oriented along one of the two shortest axes. The magnets are held together with adhesive putty so that their poles are antiparallel and perpendicular to the nonmagnetic link between them, minimizing repulsion between magnets within the same building block. When stacking the building blocks with the same orientation, the intrasheet attraction between adjacent ellipsoids is maximized. The geometry of the stacked structure is strongly dependent on the dihedral angle between the ellipsoids. In agreement with our model, this parameter controls the overall twist in the fiber. Stacked building blocks with nonzero dihedral angles spontaneously relax to helical structures, as demonstrated in the Supporting Information, Movies S1−S5. Furthermore, positive α angles induce the formation of left-handed helices, as in the calculations, which is consistent with the existence of both left- and right-handed Bauhinia seedpod bilayers.

The applicability of our model to amyloid can be assessed by analysis of experimentally determined structures. Here we consider SSNMR results for Aβ (1−42) in amyloid form [PDB: 2BEG][13] and the HET-s (218−289) β solenoid [PDB: 2RNM].[14] Analysis of the experimental data is described in detail in the Supporting Information. Initially, β strands were approximated by ellipsoids as illustrated in Figure 5a and d. We then obtained representative geometries for the building blocks

dx.doi.org/10.1021/jp4040503 | J. Phys. Chem. B XXXX, XXX, XXX−XXX

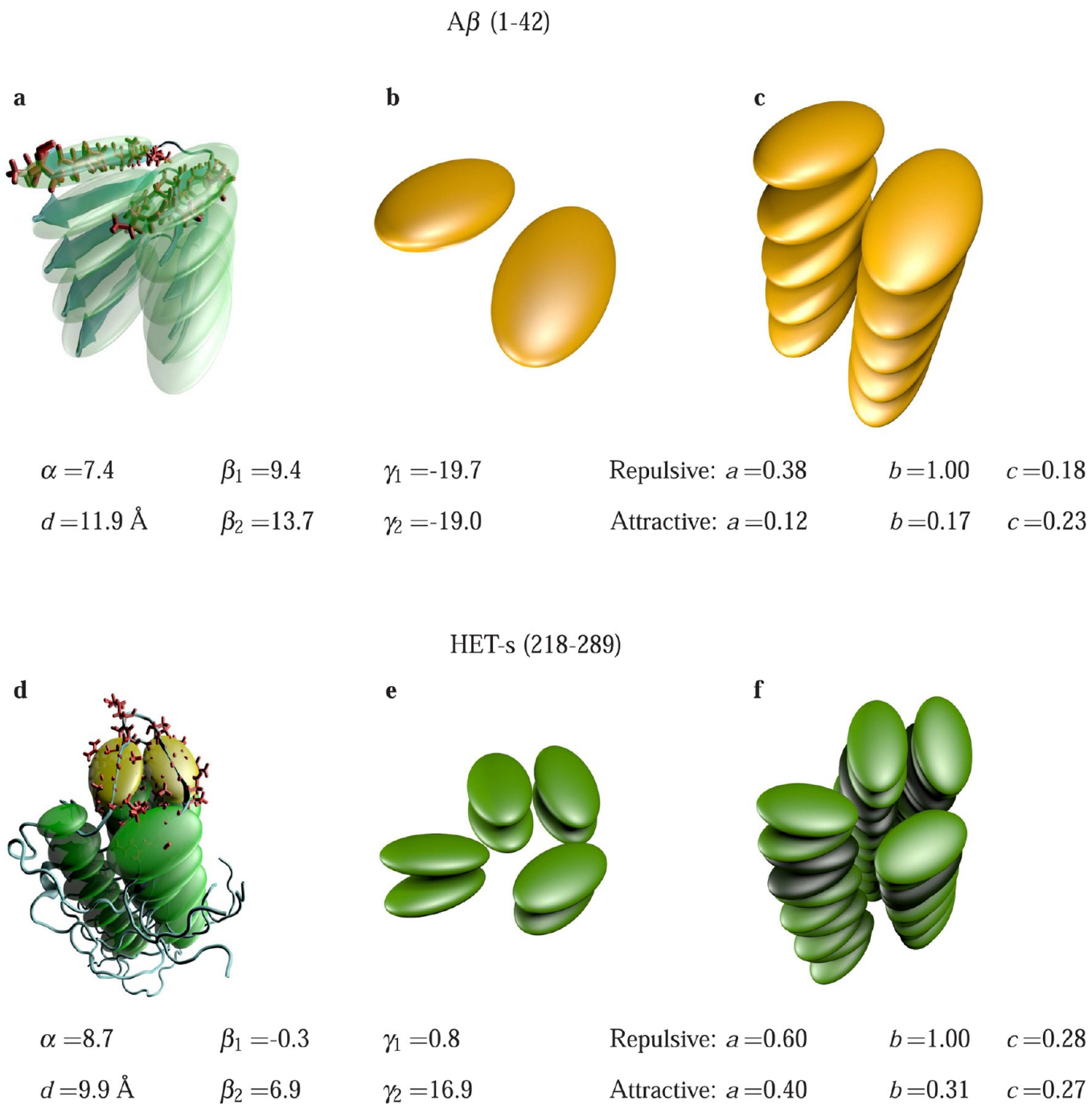

Figure 5. Graphical summary of the fitting procedure for experimental amyloid structures. (a, d) A solid elliptical prism is found with the same moments of inertia as the β strands in the fiber structure for Aβ [PDB: 2BEG][13] (top) and HET-s [PDB: 2RNM][14] (bottom). The ellipsoid inscribed within the prism defines each building block site, and the angles between the ellipsoids are given below. In the case of HET-s the values refer to the geometry of the second and third ellipsoids in the first layer of the building block (highlighted yellow). (b, e) The building block with optimized internal geometry is aligned with each set of β strands in turn to create a target structure. (c, f) Energy minimization runs are then conducted starting from a vertical stack to test how well the chosen interaction parameters between the ellipsoids reproduce the target structure. Without changing the building block geometry, optimal interaction parameters are obtained so that the energy minimized structure fits the target structure as accurately as possible. The optimal parameters for the potential are reported in reduced units, i.e., relative to the repulsive longest axis.

as BB3 for Aβ (Figure 5b) and BB4 for HET-s (Figure 5e). BB4 is more complex and consists of eight ellipsoids arranged in two layers of four, with each set of four forming a nested chevron. This representation generates a range of possibilities for assessing the frustration, but the same fundamental principles apply. A parametrization was then found for BB3 and BB4, so that the energy minimized aggregates (Figure 5c and f) matched the experimental structures as closely as possible.

The resulting best fit potential parametrization for BB3 and BB4 can be compared to BB1 and BB2. In Aβ the β strands are between seven and ten amino acids long, whereas in HET-s they vary between three and five amino acids. The ratio of the repulsive c and b axes is 5.6 for BB3 and 3.6 for BB4, which

dx.doi.org/10.1021/jp4040503 | J. Phys. Chem. B XXXX, XXX, XXX−XXX

corresponds reasonably well to the β strand lengths, confirming that the model is internally consistent. For both BB3 and BB4 the ratio of the a axis to the c axis is 2.1, which represents the ratio of the intersheet to intrasheet forces. In BB1 the ratio is 1.0, and in BB2 we set it to 0.5. Despite this wide range of values the model yields fiber structures whose morphology can be tuned simply by adjusting the internal geometry.

The effect of the greater intersheet repulsion in BB3 and BB4 is to make the structure twist less between building blocks. However, the twist is still present (Supporting Information, Figure 2). The nonzero γ values in BB3 and BB4 mean that the strongest intersheet interaction is inclined relative to the fiber axis, thereby affecting registration between the β sheets as well as the range of the interaction. For example, the center-to-center distance, d, for Aβ is 11.9 Å, or 0.43 in reduced units (Figure 5), which is larger than the value of 0.30 for BB1 and BB2. For HET-s this distance is 0.69, in part due to the shorter β strands.

The angles α, β_1, and β_2 in both BB3 and BB4 fall neatly into the range considered for BB1 and BB2. The value of α itself is similar for BB3 and BB4 (7.4° and 8.7°, respectively). However, for BB3 $\beta_1 \approx \beta_2$ and $\gamma_1 \approx \gamma_2$, and the values are quite large, which contrasts with BB4 where β_1 and γ_1 are closer to zero. Thus, the principal stack in HET-s (ellipsoid 3) is almost vertical with very little twist, with the surrounding ellipsoids generating the frustration (Supporting Information, Figure 2). The HET-s structure, which has been selected through evolution, is significantly more complex and suggests a combination of frustrated interactions, which may lead to better control over more complex long-range morphologies.

DISCUSSION

We have systematically investigated the minimal energy arrangements for internally frustrated states in pairs of interacting ellipsoids. The favored structures are bilayered helices, which possess the same range of morphologies observed in continuous frustrated bilayers and in amyloid fibers. Moreover, the same range of morphologies is observed regardless of the anisotropy of the interacting ellipsoids in the range considered, which is analogous to the independence of the morphology from the underlying material in Bauhinia seedpods.

When the internally frustrated states of these paired building blocks are stabilized, by the introduction of additional support material[4] or by kinetic trapping of conformational fluctuations,[5] our model shows that pairing in bilayers would be capable of supporting twisted ribbon, spiral ribbon, and ring-shaped morphologies, and is relatively insensitive to details of the interaction between the anisotropic units.

Previous amyloid models in which multiple β-sheets stack together face-to-face[20−22] have finite diameters and do not explain how the spiral ribbon morphology emerges due to the introduction of noncore material. Other coarse-grained models of amyloid rely on changes to the chiral or amphiphilic properties of the underlying amino acid sequence to explain the emergence of the spiral ribbon.[24] However, such fundamental properties are unaltered by the introduction of the cytochrome, and so amphilicity or chirality cannot explain the emergence of the spiral ribbon in this case.

The important novel aspect of our model is the constrained pairing of ellipsoids. Distortion of the internal assembly of the ellipsoids is capable of driving the emergence of the full range of morphologies without modifying the interaction potential at all, and thus the fiber morphology is determined almost entirely by internal frustration. Both members of the rigid pair try to assemble into the natural helical ground state that is defined by their anisotropy, but they are prevented from doing so by their rigid-body partner. The result is that the minimal energy assemblies of the internally frustrated building blocks generate long-range structures with higher energies than the helices that would be formed if the internal constraint were lifted. Thus we have shown that it may be possible to self-assemble stable macroscopic structures from discrete building blocks exhibiting internal frustration. The model makes no assumptions about the length or energy scales and is supported by an experimental realization in terms of ellipsoidal magnets.

The internal rigidity of the building blocks guarantees that both layers of the resulting bilayered filament contain the same number of ellipsoids and that the ellipsoids are all able to conserve their registration throughout the filament with their nearest neighbors. When translated into the protein domain this result means that each protein can adopt the same conformation throughout the fiber for multiple filaments, without exceeding the diameter limitation of a given filament, while adopting either twisted ribbon or spiral ribbon morphologies. In amyloid models where the β strands pack together in successive sheets[20,22] spiral ribbon morphologies cannot form, and the distortion of the outermost sheets may disrupt the alignment of the β strands, possibly requiring proteins to adopt distinct conformations throughout the fiber.

Manufacturing systems from frustrated components in practice can be complicated because one must combine the underlying components in unstable states that become stable through aggregation. To construct such materials there are at least three possible strategies, which are available at any length scale and appear to be exploited in biological systems:

1. Combine the metastable components rapidly before they can relax. This mechanism probably corresponds to the kinetics of amyloid formation.
2. Trigger internal changes after fabrication in a ground state, for example, tubule disassembly[37] due to hydrolysis of GTP bound to β-tubulin.
3. Use supplementary, possibly temporary, structures to stabilize intermediate states. Perhaps protein chaperones could be used for this function. For example, the chaperones HSP104 and HSP70 have an unknown role in the regulation of the SUP-35 prion inheritance mechanism in which SUP-35 forms an amyloid which transmits information to offspring via the conformation of the peptide, and hence the morphology of the amyloid.[38]

On the basis of insight provided by our model, we propose that there are at least three ways in which the cytochrome could change the long-range morphology from a twisted ribbon to a spiral ribbon in our experimental system:[10]

1. Cytochrome−cytochrome interactions inhibit fibrillation of twisted ribbon SH3 conformations.[4]
2. Cytochrome−SH3 interactions inhibit formation of a twisted ribbon SH3 conformation and promote formation of a spiral ribbon.
3. Longitudinal displacement of spiral ribbon subfilaments can generate apparent twisted ribbon or spiral ribbon morphologies.[12]

None of these mechanisms are mutually exclusive, and there are various experimental results that support all three. Considering the first hypothesis, after incorporation into the

dx.doi.org/10.1021/jp4040503 | J. Phys. Chem. B XXXX, XXX, XXX−XXX

fiber, only 50% of the cytochromes are able to bind heme with high affinity.[10,12] Close packing of unfolded cytochromes along the fiber backbone would explain this result, and this interpretation is supported by the fact that the morphology of the fibers changes dynamically upon takeup of heme by half the cytochromes.[12] It is also supported by the observation that the sense of the change in morphology depends on whether the cytochrome is fused to the N or C terminus of the fiber-forming SH3 domains. The complete inhibition of fiber formation upon fusion of cytochrome domains to both N and C termini is also an indicator that steric hindrance may be the mechanism at work.

Considering the second hypothesis, NMR analysis of the cytochrome-bearing fibers prior to adding heme showed that in solution only about 50% of the SH3 fiber forming domains were flexible enough to generate NMR signals, which were lost upon binding of heme, along with the signals from the cytochrome itself.[10] The NMR signals are lost because sections of the flexible polypeptide fold upon heme binding and take on the relaxation properties of the rest of the fibers, which are invisible to the NMR methods used. This result implies that some SH3 is not incorporated directly into the core of the fiber and acts as a linker region connecting the cytochrome domains to the amyloid core. That the remaining 50% of the cytochromes are not visible to NMR indicates that they clearly have limited flexibility and therefore are somehow involved with the core assembly.

The third suggestion is supported by the nature and consistency of fiber kinking, as well as the observation of changes in the position of the filament crossover points after adsorption onto mica and analysis by AFM.[12] It is entirely possible that the cytochromes displayed on the filaments within the fiber are able to interlock. If interlocking cytochromes were to misregister this could cause a kink in the fiber, where two filaments are connected in two places, but the contour length along the two filaments between the connection points is different.

The particular variant of cytochrome-bearing fibers with the highest density of kinks was the fiber made from a fusion protein containing a cytochrome domain covalently bound to the N terminus of a chain of three covalently attached SH3 domains. It is distinctly possible that in this construct there are two alternative registrations of the adjacent SH3 domains in the core and hence two different linker lengths between the core amyloid and the cytochrome domains. A random distribution of these two linker lengths would lead to defects that manifest as kinks.

These data demonstrate that our model has potential applications well beyond explaining transitions in decorated amyloid fibers. Specifically, one can conceive of higher-order assemblies in which well-defined aggregates compile into larger, possibly even bulk, systems.

In situations where the eventual morphology is driven by frustration and is independent of the anisotropic forces that drive the assembly, the defining characteristic of the eventual aggregate is the morphology itself. In such cases many distinct morphologies may exist simultaneously under identical physicochemical conditions, leading to polymorphism.[5,31] Since polymorphic structures may coexist under the same conditions, perhaps one could controllably vary the ratio of distinct polymorphs, if they could be isolated and stabilized. This control could have a substantial effect on the higher-order assembly of bulk materials, which is of interest for two reasons:

1. Higher-order frustration between the morphologically defined structures can give rise to complex higher-order behavior. For example, Bauhinia seedpods are made from *two* helical bilayers, with *opposing* chirality,[34] that mutually inhibit relaxation of the other bilayer into a helix.[9] During growth, energy accumulates within each bilayer until the locking mechanism is released, which causes the two bilayers to relax rapidly into their helical minimal energy arrangement. The sudden release of energy flings the seeds within the pod into a wide dispersal pattern. Recalling that the underlying helices themselves are caused by frustration between the two sublayers, we see that the Bauhinia seedpod actually nests two layers of frustration hierarchically. Such a simple but powerful technique can produce advanced functionality, which is approximately material and scale independent.

2. Inserting a functional group into a superstructure offers control over the morphology but also distributes nanoscopic payloads in an efficient and tunable way throughout a bulk system. Large-scale nanoscopic engineering is currently one of the most important challenges facing manufacturing. Indeed, most biological tissues are fibrous in nature, possibly for similar reasons. For example, the cytochrome decorating the fibers can bind a heme molecule, which is often used in biology as an electron transfer cofactor. Networks of such hopping sites can transport electrons over long distances.[39] Understanding and using the fiber as a scaffold for such cofactors would lead to control over the spatial distribution of the electron transfer protein, in essence generating a three-dimensional network of quantum dots under genetic control. The detailed structure of the fiber is defined with atomic resolution, even though the fiber itself is many micrometers long, providing a well-defined connection between the atomic and macroscopic domains.

The third hypothesis for the involvement of the cytochrome in driving the morphology change in decorated fibers was based on the idea that the displayed cytochromes could mediate filament realignment within a single fiber. This is precisely the kind of higher-order behavior referred to above. In previous work systematic kinking of the fibers was observed, in which certain complex long-range shapes emerged.[12] The interlocking and misregistration of decorated filaments may explain such behavior, which could be accommodated by extending the model discussed here to explicitly include hard-sphere repulsive sites to represent the cytochrome, as well as looking at multiple filament systems.

CONCLUSION

In previous work the introduction of a cytochrome domain into an amyloid fiber produced an interesting range of experimental observations that are not otherwise accessible. Three results in particular are pertinent:

1. The ability of the cytochrome to bind heme allowed dynamic adjustment of the fiber morphology.[12]
2. The interlocking of fiber filaments introduced systematic kinking.[12]
3. The transition from a twisted ribbon to a spiral ribbon morphology.[10]

We hypothesized that these results could be explained if the cytochrome frustrated the arrangement of β strands within the fiber. In the present contribution we have developed a simple coarse-grained model to explore the connection between frustration and the resulting long-range morphologies. By constructing a rigid link between two anisotropic interacting

dx.doi.org/10.1021/jp4040503 | J. Phys. Chem. B XXXX, XXX, XXX−XXX

units we have shown that the precise helical morphology of aggregates formed from such a composite building block primarily depends on the nature of the rigidification, rather than the nature of the interaction or the anisotropy of the interacting units, which is the more typical approach.[20−22,24] Our framework can be viewed as a discrete version of the bilayered frustration principle that drives the morphological transitions of the Bauhinia seedpod.

It is not immediately obvious how to manufacture an internally frustrated system using a self-assembling process, but we suggest that self-assembly may be feasible if the building blocks themselves are internally frustrated. This result would explain why misfolded proteins can nucleate fibers with distinct morphologies under the same conditions, i.e., polymorphism. Such misfolded protein conformations can be stabilized as a new ground state by introducing additional material that is not directly involved in the core of the fiber. Frustration of the fiber-forming core also provides a certain amount of control over the long-range morphology and could explain all three experimental observations mentioned above.

Reverse engineering of the potential for HET-s suggests that a wide range of noncore frustration effects are possible and that natural amyloid fibers may have evolved to exploit this frustration, perhaps in coevolution with specific chaperones, to allow the optimization of the morphology for functional fibers. From this viewpoint, amyloid appears as a molecular-scale example of a more general universal bilayered frustration principle, which could have profound implications for materials design using fibrous systems. Our model provides quantitative guidance for such applications. The relevance of this framework to longer length scales was proved by designing the morphology of a series of macroscopic magnetic stacks.

In summary, this work has led to the idea of mixing controlled morphologically defined species to generate higher-order assembly and complex functional behavior. The systematic kinking of decorated fibers and the nested frustration of the Bauhinia seedpod are two outstanding examples.

■ ASSOCIATED CONTENT

Supporting Information

A more detailed description of the angular conventions in the model, a discussion on scaling the model, and a brief summary of the method used to analyze the PDB structures. Also alternative views of the HET-S and Aβ models are provided as well as videos of the magnetic model. This material is available free of charge via the Internet at http://pubs.acs.org.

■ AUTHOR INFORMATION

Corresponding Author

*E-mail: chrisforman@cantab.net.

Notes

The authors declare no competing financial interest.

■ ACKNOWLEDGMENTS

We gratefully acknowledge funding from a CIM program grant and from the European Research Council. S.N.F. is grateful to Dr. Bela Viskolcz for helpful suggestions.

■ REFERENCES

(1) Snelson, K. Snelson on the Tensegrity Invention. *Space Struct.* **1996**, *11*, 43−48.

(2) Adhikari, R.; Skelton, R.; Pinaud, J.; Chan, W.; Helton, J. An Introduction to the Mechanics of Tensegrity Structures. *IEEE Deci. Contr. P.* **2001**, 4254−4259.

(3) Liedl, T.; Högberg, B.; Tytell, J.; Ingber, D. E.; Shih, W. M. Self-Assembly of Three-Dimensional Prestressed Tensegrity Structures from DNA. *Nat. Nanotechnol.* **2010**, *5*, 520−4.

(4) Dong, H.; Paramonov, S. E.; Aulisa, L.; Bakota, E. L.; Hartgerink, J. D. Self-Assembly of Multidomain Peptides: Balancing Molecular Frustration Controls Conformation and Nanostructure. *J. Am. Chem. Soc.* **2007**, *129*, 12468−72.

(5) Petkova, A. T.; Leapman, R. D.; Guo, Z.; Yau, W.-M.; Mattson, M. P.; Tycko, R. Self-Propagating, Molecular-Level Polymorphism in Alzheimer's Beta-Amyloid Fibrils. *Science* **2005**, *307*, 262−5.

(6) Paravastu, A. K.; Petkova, A. T.; Tycko, R. Polymorphic Fibril Formation by Residues 10−40 of the Alzheimer's Beta-Amyloid Peptide. *Biophys. J.* **2006**, *90*, 4618−29.

(7) Tschierske, C.; Nurnberger, C.; Ebert, H.; Glettner, B.; Prehm, M.; Liu, F.; Zeng, X.-B.; Ungar, G. Complex Tiling Patterns in Liquid Crystals. *Interface Focus* **2011**, *2*, 669−680.

(8) Dias, M.; Dudte, L.; Mahadevan, L.; Santangelo, C. Geometric Mechanics of Curved Crease Origami. *Phys. Rev. Lett.* **2012**, *109*, 1−5.

(9) Armon, S.; Efrati, E.; Kupferman, R.; Sharon, E. Geometry and Mechanics in the Opening of Chiral Seed Pods. *Science* **2011**, *333*, 1726−30.

(10) Baldwin, A. J.; Bader, R.; Christodoulou, J.; MacPhee, C. E.; Dobson, C. M.; Barker, P. D. Cytochrome Display on Amyloid Fibrils. *J. Am. Chem. Soc.* **2006**, *128*, 2162−3.

(11) Bader, R.; Bamford, R.; Zurdo, J.; Luisi, B. F.; Dobson, C. M. Probing the Mechanism of Amyloidogenesis through a Tandem Repeat of the PI3-SH3 Domain Suggests a Generic Model for Protein Aggregation and Fibril Formation. *J. Mol. Biol.* **2006**, *356*, 189−208.

(12) Forman, C. J.; Nickson, A.; Anthony-cahill, S.; Kaggwa, G.; Feber, U.; Sheikh, K.; Suzanne, J.; Barker, P. Towards the Control of the Morphology of Amyloid Fibres Displaying Electron Transfer Protein. *ACS Nano* **2012**, *6*, 1332−1346.

(13) Luhrs, T.; Ritter, C.; Adrian, M.; Riek-Loher, D.; Bohrmann, B.; Doeli, H.; Schubert, D.; Riek, R. 3D Structure of Alzheimer's Amyloid-Beta(1−42) Fibrils. *Proc. Natl. Acad. Sci. U.S.A.* **2005**, *102*, 17342−17347.

(14) VanMelckebeke, H.; Wasmer, C.; Lange, A.; Ab, E.; Loquet, A.; Böckmann, A.; Meier, B. H. Atomic-Resolution Three-Dimensional Structure of HET-s(218−289) Amyloid Fibrils by Solid-State NMR Spectroscopy. *J. Am. Chem. Soc.* **2010**, *132*, 13765−75.

(15) Nelson, R.; Sawaya, M. R.; Balbirnie, M.; Madsen, A. O. O.; Riekel, C.; Grothe, R.; Eisenberg, D. Structure of the Cross-Beta Spine of Amyloid-Like Fibrils. *Nature* **2005**, *435*, 773−8.

(16) Ghafouri, R.; Bruinsma, R. Helicoid to Spiral Ribbon Transition. *Phys. Rev. Lett.* **2005**, *94*, 1−4.

(17) Lugomer, S.; Fukumoto, Y. Generation of Ribbons, Helicoids, and Complex Scherk Surfaces in Laser−Matter Interactions. *Phys. Rev. E* **2010**, *81*, 1−11.

(18) Smith, B.; Zastavker, Y. V.; Benedek, G. B. Tension-Induced Straightening Transition of Self-Assembled Helical Ribbons. *Phys. Rev. Lett.* **2001**, *87*, 26−29.

(19) Fejer, S. N.; Wales, D. J. Helix Self-Assembly from Anisotropic Molecules. *Phys. Rev. Lett.* **2007**, *99*, 1−4.

(20) Knowles, T. P. J.; De Simone, A.; Fitzpatrick, A. W.; Baldwin, A.; Meehan, S.; Rajah, L.; Vendruscolo, M.; Welland, M. E.; Dobson, C. M.; Terentjev, E. M. Twisting Transition between Crystalline and Fibrillar Phases of Aggregated Peptides. *Phys. Rev. Lett.* **2012**, *109*, 158101.

(21) Aggeli, A.; Nyrkova, I. A.; Bell, M.; Harding, R.; Carrick, L.; Mcleish, T. C. B.; Semenov, A. N.; Boden, N. Hierarchical Self-Assembly of Chiral Rod-Like Molecules as a Model for Peptide Beta-Sheet Tapes, Ribbons, Fibrils, and Fibers. *Proc. Natl. Acad. Sci. U.S.A.* **2001**, *98*, 11857−11862.

(22) Adamcik, J.; Jung, J.-M.; Flakowski, J.; De Los Rios, P.; Dietler, G.; Mezzenga, R. Understanding Amyloid Aggregation by Statistical

Analysis of Atomic Force Microscopy Images. *Nat. Nanotechnol.* **2010**, *5*, 4−9.
(23) Fitzpatrick, A. W. P.; et al. Atomic Structure and Hierarchical Assembly of a Cross-θ Amyloid Fibril. *Proc. Natl. Acad. Sci. U.S.A.* **2013**, *110*, 5468−5473.
(24) Bellesia, G.; Fedorov, M. V.; Timoshenko, E. G. Structural Transitions in Model Beta-Sheet Tapes. *J. Chem. Phys.* **2008**, *128*, 195105.
(25) Dobson, C. M. Protein Misfolding, Evolution and Disease. *Trends Biochem. Sci.* **1999**, *24*, 329−32.
(26) Li, Z.; Scheraga, H. Monte Carlo-Minimization Approach to the Multiple-Minima Problem in Protein Folding. *Proc. Natl. Acad. Sci. U.S.A.* **1987**, *84*, 6611−5.
(27) Wales, D. J.; Doye, J. P. K. Global Optimization by Basin-Hopping and the Lowest Energy Structures of Lennard-Jones Clusters Containing up to 110 Atoms. *J. Phys. Chem. A* **1997**, *101*, 5111−5116.
(28) Wales, D. J.; Scheraga, H. Global Optimization of Clusters, Crystals, and Biomolecules. *Science* **1999**, *285*, 1368−1372.
(29) Wales, D. J. *GMIN: A Program for Basin-Hopping Global Optimisation*; http://www-wales.ch.cam.ac.uk/software.html (accessed November 2011).
(30) Paramonov, L.; Yaliraki, S. N. The Directional Contact Distance of Two Ellipsoids: Coarse-Grained Potentials for Anisotropic Interactions. *J. Chem. Phys.* **2005**, *123*, 194111.
(31) Pedersen, J. S.; Andersen, C. B.; Otzen, D. E. Amyloid Structure−One but Not the Same: the Many Levels of Fibrillar Polymorphism. *FEBS J.* **2010**, *277*, 4591−601.
(32) Kahn, P. C. Defining the Axis of a Helix. *Comput. Chem.* **1989**, *13*, 185−189.
(33) Efrati, E.; Sharon, E.; Kupferman, R. Elastic Theory of Unconstrained Non-Euclidean Plates. *J. Mech. Phys. Sol.* **2009**, *57*, 762−775.
(34) Rubin, N.; Perugia, E.; Wolf, S. G.; Klein, E.; Fridkin, M.; Addadi, L. Relation between Serum Amyloid A Truncated Peptides and their Suprastructure Chirality. *J. Am. Chem. Soc.* **2010**, *132*, 4242−8.
(35) Fukuma, T.; Mostaert, A. S.; Serpell, L. C.; Jarvis, S. P. Revealing Molecular-Level Surface Structure of Amyloid Fibrils in Liquid by Means of Frequency Modulation Atomic Force Microscopy. *Nanotechnology* **2008**, *19*, 384010.
(36) Madine, J.; Jack, E.; Stockley, P. G.; Radford, S. E.; Serpell, L. C.; Middleton, D. a. Structural Insights into the Polymorphism of Amyloid-Like Fibrils Formed by Region 20−29 of Amylin Revealed by Solid-State NMR and X-Ray Fiber Diffraction. *J. Am. Chem. Soc.* **2008**, *130*, 14990−5001.
(37) Weisenberg, R. C.; Deery, W. J.; Dickinson, P. J. Tubulin−Nucleotide Interactions During the Polymerization and Depolymerization of Microtubules. *Biochemistry* **1976**, *15*, 4248−54.
(38) Saibil, H. R.; Seybert, A.; Habermann, A.; Winkler, J.; Eltsov, M.; Perkovic, M. Heritable Yeast Prions Have a Highly Organized Three-Dimensional Architecture with Interfiber Structures. *Proc. Natl. Acad. Sci. U.S.A.* **2012**, *109*, 14906−14911.
(39) Page, C. C.; Moser, C. C.; Dutton, P. L. Mechanism for Electron TransferWithin and between Proteins. *Curr. Opin. Chem. Biol.* **2003**, *7*, 551−556.